RESEARCH ARTICLE



Check for updates



Observations and modeling of shear stress reduction and sediment flux within sparse dune grass canopies on managed coastal dunes

John Dickey 1,2 | Meagan Wengrove 1 | Nicholas Cohn 3 | Peter Ruggiero 4 | Sally D. Hacker⁵

Correspondence

John Dickey, Civil and Construction Engineering, Oregon State University, Corvallis, OR 97331, USA. Email: dickeyjo@oregonstate.edu

Funding information

Engineer Research and Development Center; Oregon Sea Grant, Oregon State University, Grant/Award Number: NA18OAR4170072

Abstract

Wind flow over coastal foredunes adapts to vegetation, resulting in spatial gradients in bed shear stresses that contribute to the formation of localized bedforms. Understanding, and having the capability to numerically predict, the distribution of sediment deposited within sparsely vegetated dune complexes is critical for quantifying the ecological, protective, and economic benefits of dune management activities. Data from wind tunnel experiments have indicated that there is a spatial lag from the canopy leading edge to a downwind location where sediment deposition first occurs. The length scale of this deposition lag is further quantified here using new field measurements of aeolian sediment transport across sparsely vegetated managed dune systems in Oregon, USA. We develop a deposition lag length scale parameter using both lab and this new field data and then incorporate this parameter into the process-based aeolian sediment transport model, Aeolis, which also includes a new far-field shear stress coupler. Results from numerical simulations suggest that the spatial deposition lag effect is significant for model skill in sparsely vegetated dunes. We observe with field and laboratory observations that, as canopy density increases, the length of the deposition lag decreases. As such, within the model framework the implementation of the deposition lag length does not affect the results of models of coastal dune geomorphological evolution within higher density canopies. Dune canopy density can vary due to natural (e.g., storm overwash, burial, die-off) or anthropogenic (e.g., managed plantings, dune grading) processes.

KEYWORDS

aeolian, dunes, ecogeomorphology, modeling, sediment transport

INTRODUCTION

Dunes are important geomorphic features in coastal settings because of the coastal protection benefits and other ecosystem services that they provide (Barbier et al., 2011). While wind-blown sediment transport is the primary mechanism of volumetric growth of coastal foredunes, the location and type of vegetation on the backshore play a dominant role in the spatial distribution of sediment deposition and foredune growth (Cowles, 1899; Hacker et al., 2019; Hesp, 1989; Olson, 1958; Ruggiero et al., 2018). For this reason, vegetation planting has long been incorporated into management strategies designed to stabilize and grow dunes to enhance storm protection (Houston &

Jones, 1987; Misak & Draz, 1997; Reckendorf et al., 1985), to mitigate sand inundation to private and public infrastructure (Sherman & Nordstrom, 1994), and to restore habitat for native dune communities (Pickart, 1988).

In many parts of the world, coastal dunes have been managed for stabilization through intentional planting of native and non-native vegetation (Avis, 1989; Bossard & Nicolae Lerma, 2020; Feagin et al., 2015; Gadgil & Ede, 1998; Hacker et al., 2012; Martínez & Psuty, 2008; Maun, 1998; Wiedemann & Pickart, 2004). Most studies exploring the role of vegetation in foredune geomorphology have observed the resultant dune geomorphology 15-100 years after planting (Biel et al., 2019; Bochev-van der Burgh et al., 2011;

¹Civil and Construction Engineering, Oregon State University, Corvallis, Oregon, USA

²Moffatt & Nichol, Seattle, Washington, USA

³U.S. Army Engineer Research and Development Center, Duck, North Carolina,

⁴Oregon State University College of Oceanic and Atmospheric Sciences, Corvallis, Oregon.

⁵Department of Integrative Biology, Oregon State University, Corvallis, Oregon, USA

Bossard & Nicolae Lerma, 2020; Ruggiero et al., 2018; Seneca et al., 1976; Woodhouse, 1978; Woodhouse & Hanes, 1967; Woodhouse et al., 1977). These established dunes have dense vegetation cover (% ground area obscured by vegetation as viewed from above) that often exceeds 50%. Fewer studies have focused on the morphological evolution of sparsely vegetated dunes (here, "sparse" refers to dune grass canopies with cover <50%), particularly those that have recently been planted for sediment stabilization on dunes, dunes that have been restored to remove non-native plant species, and recovering dunes that have been recently disturbed by extreme storm overwash. Managed or disturbed dunes have much lower vegetation cover and plant species richness relative to their natural or mature dune counterparts. For example, in the US Pacific Northwest, Biel et al. (2017) observed the vegetation cover within both undisturbed dunes and restoration areas where invasive beachgrasses were reduced to improve habitat for the endangered Western snowy plover. The restoration areas had relatively low vegetation cover of 4-16% 2-3 years after grass removal compared to the undisturbed sites that maintained vegetation cover, which was two- to fourfold higher. On coasts around the world, foredunes are often managed by planting regularly spaced vegetation. In the first 5 years after management action the dunes are considered to be sparsely vegetated and dune geomorphology evolves dependent on the frequency and type of management action (Bochev-van der Burgh et al., 2011; Bossard & Nicolae Lerma, 2020; Feagin et al., 2015; Jackson & Nordstrom, 2011). Additionally, storm overwash can also lead to reductions in vegetation abundance. Miller et al. (2009) noted that historical decreases in species richness was correlated with storm inundation from hurricanes on the Florida Gulf Coast.

Several numerical models that implement biophysical feedbacks between sediment and vegetation can produce dunes that range from hummocks to linear foredunes. One model, the Coastal Dune Model, simulates landform evolution over decades and demonstrates how zonation of dune grasses controls maximum foredune height (Durán Vinent & Moore, 2015; Moore et al., 2016). Goldstein et al. (2017) further suggest that lateral growth rates of vegetation controls the time for hummocky foredunes to coalesce into linear hills of sand. On seasonal timescales, beach-dune evolution models couple nearshore morphodynamic and ecological feedback processes into a holistic framework. XBeach-Duna (Roelvink & Costas, 2019), DUBEVEG (Keijsers et al., 2016), and Windsurf (Cohn et al., 2019) couple models to simulate aeolian transport (e.g., Aeolis), sediment trapping by vegetation and dune growth (e.g., the Coastal Dune Model), and marinedriven transport (e.g., XBeach) on a seasonal timescale. However, the implementation of biophysical feedbacks using ecological characteristics leading to sediment trapping and geomorphologic evolution of dunes is still rather crudely implemented in these ecomorphodynamic numerical models, partly because the physical mechanisms by which sediment flux is influenced by vegetation are not totally understood. Sediment transport rates through canopies of vegetation has been shown to be modified by physical interaction between the sediment and plants (Gillies & Lancaster, 2013; Hendriks et al., 2008), shear stress partitioning (Raupach, 1992; Raupach et al., 1993), and reductions in turbulent kinetic energy (Yang et al., 2016).

Regardless of the specific mechanism, wind tunnel and field studies have elucidated important relationships between arrays of roughness elements and the sediment flux at different distances downwind from the canopy leading (upwind) edge. The wind tunnel study by

Buckley (1987) measured sediment fluxes within canopies of real vegetation with cover ranging from 0 to 17% and found the sediment flux could be well predicted by a Bagnold-type transport model modified to include the cover. The field studies conducted by Gillies et al. (2006) found that the sediment flux decreased exponentially with distance into a canopy of 5-gallon buckets in an open sandy bed before reaching a limit related to the roughness density (the frontal area perpendicular to flow divided by the ground area) (Gillies & Lancaster, 2013; Gillies et al., 2006, 2015, 2018).

In addition to the spatial modifications of sediment flux caused by an array of roughness elements, the variability in growth form and morphology of dune plants also largely controls differences in sand deposition and characteristic foredune shapes due to the aggregate effects of individual plants on the sediment trapping across the dune face (Biel et al., 2019; Charbonneau and Casper, 2018; Charbonneau et al., 2021; Hacker et al., 2012, 2019; Hesp, 1989; Ruggiero et al., 2018; Seneca et al., 1976; Woodhouse and Hanes, 1967; Woodhouse et al., 1977; Zarnetske et al., 2012, 2015). In a wind tunnel study that used three dune grass species, Zarnetske et al. (2012) explored species-specific differences in sediment capture efficiency and sediment bedform growth response over a 1 m² patch of vegetation. Zarnetske et al. (2012) found that species with a higher amount of above-ground biomass exhibit higher sediment capture efficiency on an individual basis; however, species that respond to burial by producing a higher density of vertical shoots trap more sand overall. Hacker et al. (2019) showed that the actual growth form and morphology of the dune grass species, including the above-ground shoots (consisting of stems, leaves, and inflorescences) and the below-ground rhizomes (consisting of roots and stems) affect the size and shape of the resulting geomorphology.

In numerical models that simulate biophysical feedbacks between sediment and vegetation, canopies of vegetation are described in terms of their stem density (# stems/m²) and/or in terms of their vegetation cover (Cohn et al., 2019; Durán & Herrmann, 2006; Durán & Moore, 2013; Durán Vinent & Moore, 2015; Keijsers et al., 2016; Luna et al., 2011; Roelvink & Costas, 2019). While both stem density and vegetation cover represent a quantity of biomass per unit area, it is important to note that they represent slightly different properties of the vegetation field. However, in terms of sediment trapping, both high stem density and high vegetation cover are correlated with increased sediment trapping.

Lee and Soliman (1977) found that different vegetation covers result in different flow regimes including: (1) isolated roughness, where individual plants create their own wakes (cover < 16%); (2) wake interference, where the wakes of multiple plants begin to interact (16% < cover < 40%); and (3) skimming flow, where flow skims across the top of the canopy (cover > 40%). Hesp et al. (2019) utilized wooden dowels and zip ties to mimic vegetation. The mimics were used to investigate the effect of vegetation cover and plant height on boundary layer adjustment and sedimentation in both field and wind tunnel environments. They varied vegetation percent cover to test isolated roughness, wake interference, and skimming flow regimes within a wind tunnel and found that decreasing vegetation cover leads to wider, flatter, volumetrically smaller bedforms where the windward bedform toe is formed at increasing distance downwind from the canopy leading edge as the vegetation cover decreases. They also found that canopies within the skimming flow regime resulted in bedform deposition that occurred immediately at the canopy leading edge and were larger in volume and height than the canopies with less vegetation cover. These results agree with those of Charbonneau and Casper (2018), who similarly found that lower stem density resulted in deposition trailing downwind of canopies of American beachgrass Ammophila breviligulata. In terms of plant growth form, species that spread further laterally and are more evenly spaced create shorter and wider morphological bedforms, while species that are dense and clumped, with more vertical growth, create taller and narrower morphological bedforms (Hacker et al., 2019). However, it is important to keep in mind that the influence of stem density on the amount of sediment deposition around plants varies considerably between and within a single species, depending on the geographic setting (Charbonneau & Casper, 2018; Charbonneau et al., 2021; Hesp, 1981; Hesp et al., 2019). Additionally, sediment deposition among canopies of vegetation is not only a function of species growth form/ morphology and stem density. Wind tunnel studies and field observations of dune grass show that the width of a dune grass patch, angle of repose of the sediment, and wind speed provide additional controls on the sediment depositional zone length and height (Hesp, 1981).

Investigations of the adjustment of flow in forests, crops, and aquatic vegetation canopies report scaling arguments to describe the length scales for boundary layer adjustment upwind and downwind of the canopy leading edge and downwind of the canopy trailing edge (Belcher et al., 2003, 2012; Brunet et al., 1994; Chen et al., 2013; Munro & Oke, 1975; Nepf, 2011; Zong & Nepf, 2010). The canopy drag length, L_c (Figure 1) describes the distance required for the mean flow to adjust to the presence of vegetation. As the stem density increases, Lc will decrease (Belcher et al., 2003; Rominger & Nepf, 2011). By measuring the wind field upwind and through the canopy, Hesp et al. (2019) also showed that the wind speed decelerated and flow penetration decreased with increasing stem density. While Hesp et al. (2019) report the distance into the canopy for wind speed to fall below 50% of its incident value, they do not provide an analytical method, like L_c , for characterizing the vegetation cover dependent spatial pattern in wind speed attenuation.

Even though qualitatively the relationship between vegetation cover and sediment trapping is widely observed, there remains limited computational/empirical/analytical approaches to simulate the biophysical process. In this study, our goal is to develop a robust quantitative framework to predict deposition within sparsely planted dune

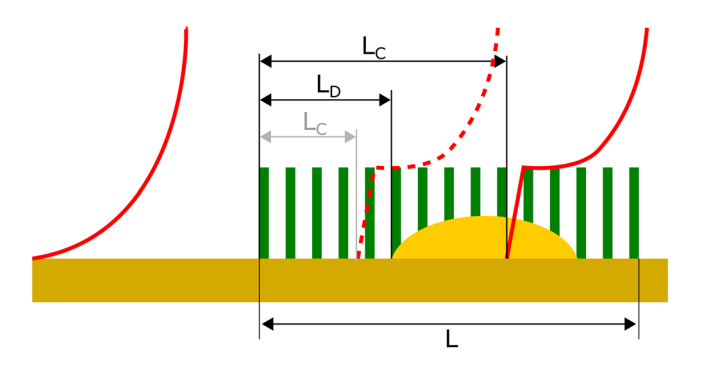


FIGURE 1 Schematic of the canopy drag length scale L_c and the deposition lag length scale L_D for wind blowing left to right over a canopy length L. The red curves represent the idealized boundary layer as it adjusts to the canopy. L_c can be smaller or greater than L_D [Color figure can be viewed at wileyonlinelibrary.com]

grass canopies. First, we observed the sediment flux through sparsely planted dune grass canopies within three dune management sites in Oregon, USA. We then used the published laboratory dataset of Hesp et al. (2019) and our field observations to propose a new empirical model for sand deposition within sparsely vegetated dunes. To do this, we determined a vegetation cover dependent deposition lag length, L_D , as a function of L_c (Figure 1). L_D describes the distance between the leading shoot and the start of the downwind depositional zone within sparse dune grass canopies. We implement L_C and LD within a shear stress partitioning framework for flow reduction within the canopy because shear partitioning is the approach used by the aeolian sediment transport model, Aeolis (Hoonhout & de Vries, 2016). We modify Aeolis to include L_D and to additionally incorporate a new shear stress partitioning reduction scheme that specifically considers sparse vegetation. Following the incorporation of these datainformed parameterizations into Aeolis, the model is used to numerically simulate spatial patterns in sediment transport and morphological growth in the presence of sparsely planted dune grass canopies of vegetation.

2 | METHODS

2.1 | Field sites, observations, and metrics

Field observations were made at three managed dune sites on the Oregon coast in July 2021. The dunes at these sites were graded by homeowners to maintain coastal views and were subsequently replanted. Two sites were in Pacific City, OR (C10 and C17), and the third was in Bayshore, OR (C21). The two sites in Pacific City were graded in fall 2020 and replanted with dune grasses per state regulation. At site C10, the stem density was 43 stems/m² and at site C17 it was approximately 121 stems/m². At Bayshore (C21), the dune was graded and replanted with dune grasses in fall of 2018. The dune grasses had several seasons to establish after planting and had a stem density of 278 stems/m² at the time of our observations (2021). The dune grass canopies at all three sites were predominately populated with European beachgrass *Ammophila arenaria*, though there was also some native American dune grass *Elymus mollis* at site C10.

In fall 2021, we established one shore perpendicular transect at each site to collect various vegetation, meteorological, and sediment measurements to be used in our models (see Table 1 for a list of the metrics measured). The vegetation surveys involved measuring vegetation cover, stem density (stems per 0.25 m²), and stem height (cm; measurements were made of both stretched and relaxed stems) of dune grasses present in 0.25 m² quadrats placed 2 m along the length of the transect (see Hacker et al., 2012, 2019, for methods). For calculation of the solid volume fractions, ϕ (see Section 4), we used the average shoot width (b_{shoot}) of 3.9 mm from Zarnetske et al. (2012) and the average shoot thickness (t_{shoot}) was assumed to be 1 mm.

To measure event scale spatial variability in wind speed and sediment flux, we deployed instruments in a transect aligned with the wind direction, stretching from the canopy leading edge to a distance of 18 m downwind of the canopy leading edge (Figure 2). The transect alignment was estimated by observing the heading of wind-aligned survey flags and was assumed to remain constant for the duration of each deployment, which lasted for 6 h (see Supporting Information

TABLE 1 Summary of the meteorological, sediment, and vegetation measurements along the three transects (C10, C17, and C21) during the deployments in July 2021 at Pacific City and Bayshore, OR

Site name	Pacific City	Pacific City	Bayshore
Transect name	C10	C17	C21
Measurement date	Jul 10 2021	Jul 9 2021	Jul 12 2021
Mean wind speed (m/s) (mean \pm SD)	4.37 ± 0.01	$\textbf{3.14} \pm \textbf{0.01}$	$\textbf{3.75} \pm \textbf{0.01}$
Mean wind direction (mean \pm SD)	$311^{\circ}\pm10^{\circ}$	$308^{\circ}\pm12^{\circ}$	$319^{\circ}\pm16^{\circ}$
Transect heading	310°	320°	330°
Sediment grain size D50 (μm)	225	229	219
Average bed level change (cm)	$\textbf{0.1} \pm \textbf{0.20}$	-0.1 ± 0.6	$\textbf{0.1} \pm \textbf{0.2}$
Maximum sediment flux (kg/m/s)	5.40E-04	2.20E-05	7.30E-04
NSF @ $x = 18 \text{ m}$	8.6E-02	2.2E-01	1.5E-02
L _c (m)	1.5	0.4	0.2
L _D (m)	7.9	1.9	0.4
Beach width (m)	150	150	60
Grass species	AMAR, ELMO	AMAR	AMAR
Vegetation cover (%)	10.0 ± 5.0	17.2 ± 7.5	20.6 ± 8.8
Stem density (stems/m²)	43.1 ± 34.5	$\textbf{121.3} \pm \textbf{89.7}$	278.2 ± 152.8
Stretch height (cm)	$52.5\pm.0.3$	58.6 ± 0.3	69.0 ± 1.5
Relax height (cm)	41.0 ± 0.3	51.3 ± 0.4	$\textbf{50.6} \pm \textbf{0.1}$

Note: The transect heading refers to the alignment of the transect at each site. Wind speed and direction are from anemometers 10 cm above the sediment surface. Beach width is estimated from GPS RTK backpack measurements collected during the deployments. The beach width is calculated as the distance between 2.1 m above NAVD88 (elevation of mean high water), and the estimated dune toe location. The dune grass species are abbreviated as: AMAR Ammophila arenaria and ELMO Elymus mollis.

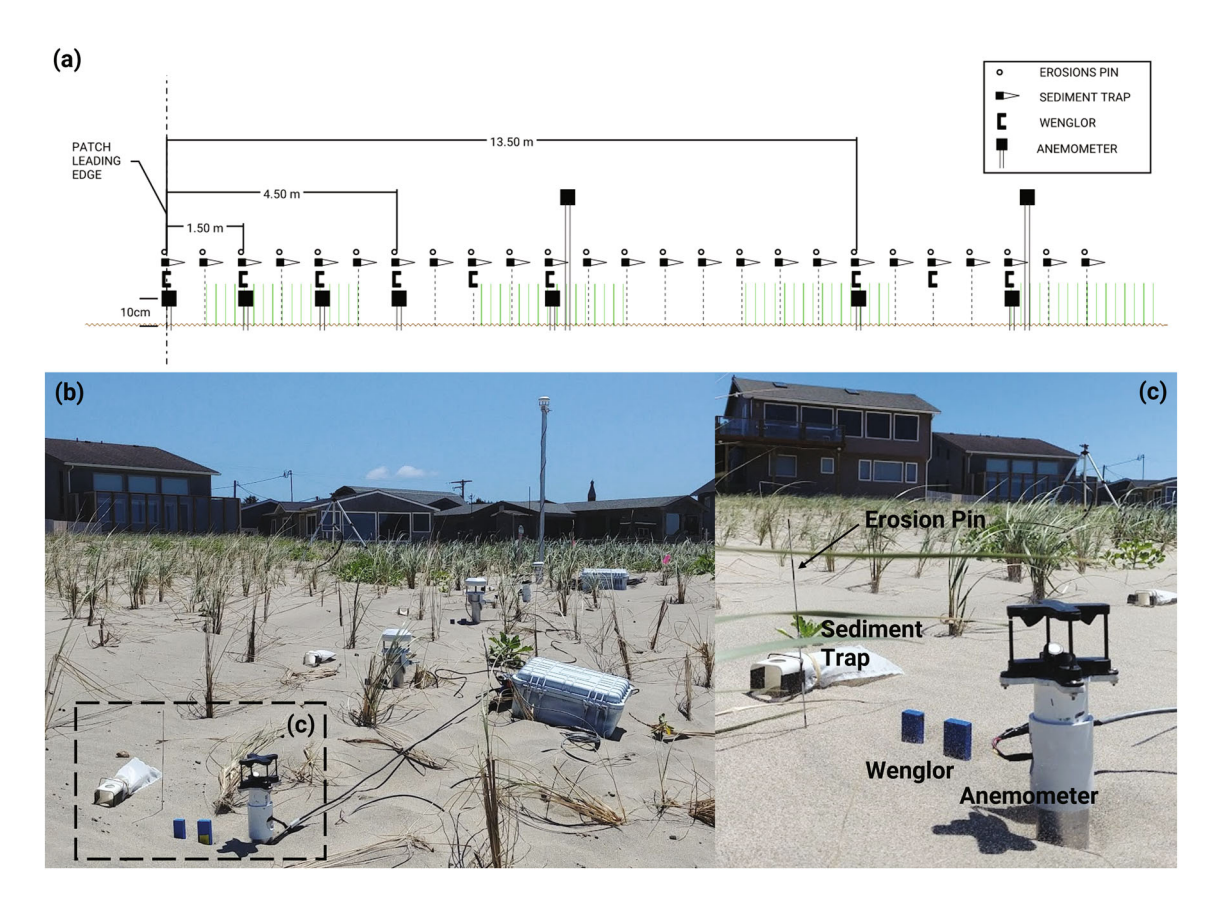


FIGURE 2 Setup for the field observations showing the instrument deployment schematic (a), image of the instrument array from an upwind position (b), and close-up of the typical instrument cluster including an anemometer, a Wenglor pulse counter (data not used), a sediment trap, and an erosion pin (c). The white box is the enclosure for our data acquisition unit. Photo taken at Pacific City, OR, on transect C10 [Color figure can be viewed at wileyonlinelibrary.com]

station is shown in Figure 2c.

Owing to limitations in the number of instruments available for this study (four Decagon DS-2 anemometers, two Meter ATMO22 and six Wenglor pulse counters) it was not possible to deploy enough measurement stations to take simultaneous measurements across the entire 18 m long transect at a sufficiently fine spatial scale to assess the length of L_D . As a result, we deployed full measurement stations at 0, 1.5, and 3 m along the transect because that captured the probable length of L_D based on the results of the Hesp et al. (2019) wind tunnel study. To cover distance further downwind, two full measurement stations and a partial measurement station (without anemometer) were located at 4.5, 6, and 7.5 m for the first half of the deployment (hours 0-3). These measurement stations were relocated to 13.5, 15, and 16.5 m for the second half of the deployment (hours 3-6). To ensure that the wind conditions were consistent for the two halves of the observation period, an anemometer was also placed on a 1.6 m tall mast. This mast was initially located at 7.8 m for the first half of the observation period and then moved to 16.8 m for the second half. The location of all instrumentation is detailed in Figure 2a. All anemometers were logged using Campbell CR6 data loggers at a sample frequency of 0.5 Hz.

To determine the spatial and temporal patterns in near-bed sediment flux, mesh-style sediment traps (similar design to Sherman et al., 2014) and erosion pins were deployed every 0.75 m along the transect to a downwind distance of 18 m (Figure 2a). The bed level was measured using the erosion pins at the beginning and end of the observation period. The average bed-level change across the transect was calculated by averaging all of the bed-level changes along the transect. The transect average bed-level change is provided for the three field observation sites in Table 1. The sediment traps were constructed of a PVC frame with a fine mesh covering. The trap openings were 3.7cm × 3.7cm and were installed flush with the bed and open in the direction of the wind (Figure 2c). Sediment traps were emptied hourly but remained in the same location and orientation for the entire deployment. Sediment trap samples were bagged and then dried, weighed, and sieved using a mechanical shaker (ASTM D6913/ D6913M-17) to determine the median grain size (D_{50}) used in the model (see Table 1). The total sediment flux per unit width measured by the sediment traps was estimated as

$$q_{\text{trap}} = \frac{M}{W_{\text{trap}}T},\tag{1}$$

where M is the total observed mass, W_{trap} is the trap width, and T is the total time that the traps were deployed. We chose to represent sediment flux measurements in units of kg/m/s because these are the units from the process-based model, Aeolis. By converting our observations to the same units, the two estimates are more easily compared. It should be noted that the relatively short vertical height of the sediment trap measurements makes it unlikely that the sediment flux was fully integrated in the vertical direction. As a result, these

sediment flux values may only capture the majority of flux (as visually observed), but not all the sediment flux moving through the transect.

2.2 Aeolis model and calibration

The influence of vegetation on dune geomorphology is typically parameterized by modifying the shear stress imparted to the sediment bed within the canopy using a shear coupler. A shear coupler is a mathematical expression used to parameterize the reduction in bed shear stress due to sheltering in vegetation or other flow obstructions. The shear stress reduction is usually characterized by the ratio of the bed shear stress in the sheltered case, $u_{*,\mathrm{veg}}$, to that of the nonsheltered case, $u_{*,o}$. One of the most widely used shear couplers in process-based aeolian sediment transport modeling is the approach developed by Raupach (1992) and Raupach et al. (1993) that parameterizes the shear reduction over a unit area by

$$\frac{u_{*\text{veg}}}{u_{*\text{o}}} = \frac{1}{\sqrt{1 + \Gamma \rho_{\text{veg}}}},\tag{2}$$

where Γ is a roughness parameter and ρ_{veg} is the vegetation cover fraction. Typically, a Γ of 16 is used for dune grasses (Durán & Herrmann, 2006).

While the Raupach shear coupler is widely used (de Vries et al., 2014; Durán & Moore, 2013; Hoonhout & de Vries, 2016; Roelvink & Costas, 2019; Van Westen, 2018) it does have a number of limitations, including a lack of accounting for irregular roughness elements such as vegetation and the non-uniform distribution of roughness elements across a surface. Rather, the model assumes that a single large roughness element can reduce bed shear stress to the same degree as many small roughness elements scattered across the surface. Additionally, the Raupach shear coupler does not resolve the sheltering that occurs in the region downwind of a roughness element.

An alternative model for shear stress reduction developed by Okin (2008) parameterizes the sediment flux in vegetated regions by accounting for the spacing between plants. Okin's expression for the shear reduction of a single plant is given by

$$\frac{u_{* \text{veg}}}{u_{* 0}}(x) = R_0 + [1 - R_0] \left[1 - \exp\left(-c\frac{x}{h}\right) \right], \tag{3}$$

where $R_0 = u_{*,veg}/u_{*,o}$ at x = 0, the coordinate x is relative to the roughness element, c is a factor controlling the rate at which shear stress recovers with distance, and h is the height of the roughness element. Okin (2008) originally proposed $R_0 = 0.32$ and c = 4.8 based on fitting an exponential curve to observations made by Bradley and Mulhearn (1983), of bed shear stress recovering in the lee of a sand fence. The advantage of the Okin shear coupler formulation is that it attempts to resolve the spatial gradient in shear stress in the lee of roughness elements. Additionally, R₀ and c are parameters used to adjust the influence of the roughness elements on bed shear stress and can be estimated via wind tunnel studies or the deployment of anemometer arrays in the field.

Both shear couplers predict shear reduction immediately at the canopy leading edge where flow first encounters the vegetation. For sparse dune grass canopies, the results of Hesp et al. (2019) suggest that the full shear reduction from the canopy may not occur until some distance downwind from the canopy leading edge. Belcher et al. (2003) proposed the length scale, L_c , to represent the distance for flow to adjust to the canopy:

$$L_c = \frac{2(1-\phi)h_c}{C_D\lambda}, \tag{4}$$

where ϕ is the canopy solid volume fraction, h_c is the canopy height, λ the plant frontal area per unit bed area (m²/m²), and C_D is the stem scale drag coefficient. We approximate h_c as the relaxed height of the vegetation, $h_{\rm relax}$. $\lambda = \alpha N_{\rm shoots} b_{\rm shoot} I$ where α is the ratio of the number of blades per grass stem, $N_{\rm shoots}$ is the canopy density, $b_{\rm shoot}$ is the shoot width, and I is the length of the shoot estimated by $h_{\rm stretch}$, the stretched height of the grass measured from the bed to the top of the longest shoot. The solid volume fraction, ϕ , is the fraction of a unit volume occupied by vegetation. $\phi = \alpha N_{\rm shoots} b_{\rm shoot} t_{\rm shoot} (h_{\rm stretch}/h_{\rm relax})$, where $t_{\rm shoot}$ is the average shoot thickness and $b_{\rm shoot}$ is the average shoot width. The stem scale drag coefficient, C_D , was estimated per Rominger and Nepf (2011) by using the stem diameter and the wind speed measured by the anemometer at the canopy leading edge to calculate the Reynolds number, Re. The expression for C_D from Rominger and Nepf (2011) is $C_D = 1 + 10 \text{Re}^{-2/3}$.

The shear coupler suggested by Raupach et al. (1993) has previously been implemented to account for vegetation–wind–sediment interactions in simulations of the morphological evolution of coastal foredunes. Aeolis (Hoonhout & de Vries, 2016) is a process-based aeolian transport model that includes the detailed effects of surface moisture, sediment armoring, and vegetation on wind blown sediment transport (e.g., Van Westen, 2018). Herein, the modular and open-source Python code of Aeolis is adapted to include new approaches for incorporating the Okin shear coupler, L_c , and L_D to better mimic the effects of sparse vegetation on modifying bed shear stresses adjacent to and in the lee of plants and vegetation canopies.

The first set of Aeolis simulations were applied to the published Hesp et al. (2019) wind tunnel cases, which provide information on bed elevation changes for canopies subject to wind forcing that varied in percent vegetation cover. The models were forced using their reported wind speed. The vegetation mimics were reported to have blade widths (b_{shoot}) of 4 mm with 4 blades/plant (α). We assumed a blade thicknesses (t_{shoot}) of 1 mm. The parameters for the Raupach and Okin shear couplers were tuned using the model runs that best simulated the volume of the deposition zone in the 51% and 38% cover cases from the Hesp et al. (2019) dataset. The remaining vegetation density cases (12% and 23%) were used to evaluate the model behavior using the Raupach and Okin shear couplers and additionally with implementation of L_D . We modified Aeolis by implementing a model for L_D based on the empirical relationship with L_c fitting the Hesp et al. (2019) dataset and separately fitting our field observations. The methods for implementing L_D are described in further detail below and the derived formulation for LD based on the various field and laboratory datasets are provided in Section 4.

Additional 1D simulations were completed to model the sediment transport rates and patterns at Pacific City, OR, and Bayshore, OR, for the same time periods where field data were available. In general, the formation of coastal dunes is dependent on complex 2D and 3D processes. However, we decided that a simplified 1D model would allow

for simple comparison with the Hesp et al. (2019) dataset. Additionally, the choice of a 1D model is justified because the wind directions were well aligned with our transects such that a majority of the sediment flux occurred along this alignment and the short duration of the observed wind events (6 h) reduced the possibility of wind-sediment feedback process causing significant changes in the bed morphology. The transect alignment, average wind direction, and average bed-level change are provided in Table 1. All Aeolis simulations were set up with the grain sizes and vegetation parameters listed in Table 1. The model setup assumes vegetation cover can be reasonably approximated by uniformly spaced shoots; while managed dune plantings are typically regularly spaced at the time of establishment, this condition will change over time as a result of growth and expansion of the grasses. The models of the field observations were forced with a time series of 30 s averaged near-bed upwind anemometer observations from the anemometer located at x = 0 m in Figure 2.

To estimate sediment transport in the Aeolis simulations, the modified Bagnold sediment flux formulation (Bagnold, 1937)

$$q_{\text{,Bagnold}} = C_b \sqrt{\frac{D_{\text{sed}} \rho}{D_{\text{ref}} g}} (u_* - u_{*,\text{th}})^3, \tag{5}$$

is used to produce the model fluxes, where u_* is the friction velocity from the wind forcing, $u_{*,\text{th}}$ is the threshold friction velocity, D_{sed} is the average grain size, D_{ref} is the reference grain size (taken here to be 0.25 mm), ρ is the density of air, g is the acceleration due to gravity, and C_b is a model coefficient typically related to the grain size distribution. Within Aeolis, u_* is calculated from the wind forcing via Prandtl–Von Kármán's law of the wall, where the roughness height, z_0 , is determined by the grain size following Sherman (1992). Unless otherwise noted, C_b is set to 1.5. u_* th is typically calculated as

$$u_{*,th} = A \sqrt{gD_{sed} \frac{\rho_s - \rho}{\rho}},$$
 (6)

where A is a coefficient of 0.08 for the dynamic threshold governed by saltation impact forces and ρ_s is the density of the sediment. Ignoring any supply limiting conditions, Equation (5) will produce the equilibrium sediment concentration within Aeolis. The modeled sediment fluxes are compared to the observed sediment trap measurements by computing the time averaged flux over the duration (T) of the simulation

$$q_{\text{obsv}} = \frac{1}{T} \int_{t=0}^{t=T} q(t) dt.$$
 (7)

We also utilized the normalized sediment flux (NSF), as described by Gillies et al. (2006), where the observed sediment flux values are normalized by the sediment flux entering the canopy. Applying the NSF to the field observations and model predictions allows us to assess the spatial patterns in sediment flux attenuation without needing to calibrate the model to exactly match the sediment fluxes observed in the field. This is useful because our sediment trap instruments are unlikely to capture the entire sediment flux. However, we did observe most sediment flux to be moving at bed level where our traps were located, so we likely do measure a majority of the flux.

The Hesp et al. (2019) dataset is used to calibrate the performance of the shear couplers and the empirical expression proposed for L_D . Hesp et al. (2019) do not provide information on the sediment flux entering the mimic canopies; therefore, we calibrated the models using the reported bedform volumes in that publication. Additionally, Hesp et al. (2019) did not quantitatively define the relationship between the canopy density and the location of the bedform toe; therefore, we defined the distance from the canopy leading edge to the bedform toe as the deposition lag length scale, L_D (Figure 1). L_D was transcribed from fig. 18 in Hesp et al. (2019) as 100, 70, 30, and 2 cm downwind from the 12%, 23%, 38%, and 51% cover cases, respectively.

The 51% cover case was used for calibration of the Aeolis simulations because the observed L_D was small (2 cm), so sediment trapping due to vegetation occurred almost immediately as the flow entered the canopy, which is the inherent assumption of the shear couplers without LD implementation regardless of vegetation cover. In the simulations, the overall transport was adjusted by increasing the C_b in Equation (5) until the volume of sediment trapped in the model using the Raupach shear coupler was within 1% of the volume reported. In addition to the downwind translation of the sediment deposition zone with decreasing vegetation cover, Hesp et al. (2019) observed a significant decrease in bedform volume as the cover decreased below 51%. To account for the step change in observed deposition morphology we use different sets of values for R_o and c in Equation (3) depending on vegetation cover, corresponding to whether the system is within or outside the skimming flow regime. The values of R_0 and c were found by minimizing the error between the modeled and observed dune volume. For vegetation cover > 40% (skimming flow regime) the coefficients were found to be $R_0 = 0.47$ and c = 5.0. For canopies with cover less than the skimming flow regime, the 38% vegetation cover case was used for calibration, resulting in $R_0 = 0.94$ and c =0.87.

 L_D is implemented in Aeolis by preventing the vegetation from reducing the bed shear stress in the adjustment region defined between the canopy leading edge and a distance L_D downwind. We use L_D to mask the operation of the shear coupler (i.e., Equations 2 and 3) such that no shear reduction and associated deposition occur within the adjustment region bound between the canopy leading edge and a distance L_D downwind of the leading edge. The empirical expression found from the linear regression between L_D and L_c is used to calculate $L_{D, \text{empirical}}$ (see Results). To prevent unrealistic behavior from the use of this empirical model we enforce restrictions on L_D such that

$$L_{D} = \begin{cases} 0, \text{if } L_{D, \text{empirical}} < 0, \\ L_{D, \text{empirical}}, \text{if } 0 < L_{D, \text{empirical}} < L, \\ L, \text{if } L_{D, \text{empirical}} \ge L, \end{cases} \tag{8}$$

where L is the length of the canopy.

2.2.1 | Statistics for comparing model results

The Brier skill score (BSS), also known as the mean squared error (MSE) skill score (Murphy, 1988), is a commonly used method for evaluating the skill of geomorphic models (Sutherland et al., 2004). We

use the BSS to compare how each combination of model modifications performed relative to a reference model in terms of the mean square error calculated as

$$MSE = \frac{1}{N} \sum_{i=1}^{N} (P_i - O_i)^2,$$
 (9)

where *P* are the model predictions and *O* are the observations. The BSS is calculated from the MSE as

$$BSS = 1 - \frac{MSE_i}{MSE_{ref}}, \tag{10}$$

where MSE_i is the MSE associated with the model modifications (e.g., Okin, Raupach with L_D , and Okin with L_D). MSE_{ref} refers to the MSE of our reference model. We chose the reference model to be Aeolis running with the Raupach shear coupler without L_D so that we could evaluate how our model modifications improved the model skill relative to the standard approach. Possible skill scores range from 1 to $-\infty$, with positive numbers indicating an improvement relative to the reference model and negative numbers indicating predictions worse than the reference model. In this study we compute BSS values based on time-averaged sediment fluxes, changes in bed elevation, bedform volume, and bedform position, which is characterized by the horizontal position of the bedform toe, crest, centroid, and heel.

3 | RESULTS

We first present results from field observations that measure sediment flux through varying stem densities in managed Oregon dunes. Then we use the Hesp et al. (2019) wind tunnel experiment observations along with our field observations to test the Raupach and Okin shear couplers and our new empirical formulation for L_D . We then use the shear couplers and L_D to replicate the sediment fluxes from the field observations.

3.1 | Field observations

A summary of the meteorological, sediment, and vegetation measurements along the three transects (C10, C17, and C21) is given in Table 1. We computed the long-term average wind speed by taking the average of the time series from each near-bed anemometer over the entire duration of the instrument's deployment (Table 1). We observed that the predominant wind direction varied between the mast (above canopy) and near the bed (canopy height) wind speed measurement positions by up to 20° . The observations of wind direction at the top of the mast suggest that the orientation of the transects was nearly in line with the dominant wind direction. Additionally, our visual observations of vegetation streaming orientation and active saltation direction suggest that the sediment transport direction was reasonably well aligned with our transects. As such, the near-bed wind direction measurements from the anemometers were likely influenced by the vegetation canopy.

The variability of the time-averaged wind speed and sediment flux across transects shows a clear upwind migration of the point of

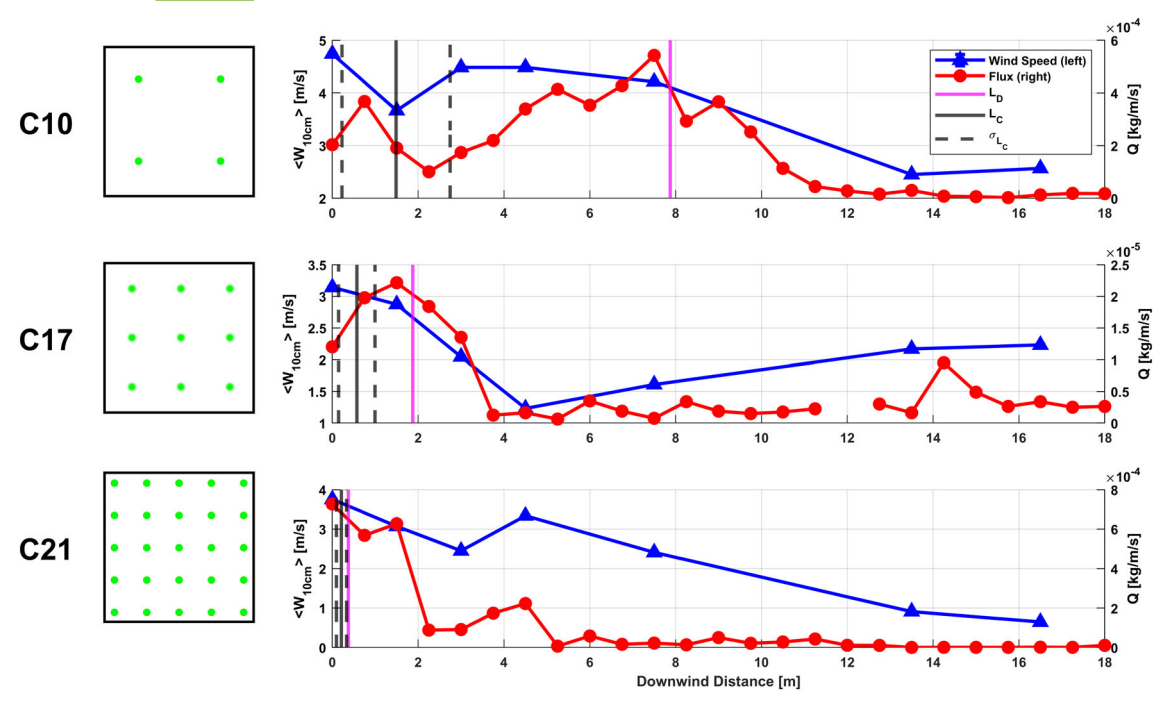


FIGURE 3 Summary of the wind speed (blue line with triangle markers) and sediment flux (red line with circle markers) attenuation along the three transects (C10, C17, and C21) with varying vegetation covers and stem densities (boxes to the left of each plot). L_c (gray line) and L_D (magenta line) are also plotted for the three transects. Note that transect C10 (top panel), which has the lowest vegetation cover, is within the isolated roughness regime and that transects C17 and C21 (middle and bottom panels), each with greater vegetation cover, are within the wake interference regimes [Color figure can be viewed at wileyonlinelibrary.com]

maximum sediment flux as the vegetation cover and stem density increase (Figure 3). As vegetation cover and stem density increase, the attenuation of both wind speed and sediment flux occur further upwind. The wind speed is attenuated by a maximum of 48% at 13.5 m, 61% at 4.5 m and 83% at 16.5 m downwind for transects C10, C17, and C21, respectively. The downwind recovery of the wind speed for transect C17 is likely caused by more onshore alignment of the wind field as the experiment progressed. Similarly, the sediment flux is attenuated below 90% at 12.75, 5.25, and 5.25 m downwind of the canopy leading edge for transects C10, C17, and C21, respectively. Table 1 shows the sediment flux at the furthest downwind sampling location (i.e., 18 m) for each transect.

We observed that L_D varied with stem density, vegetation cover and wind speed. The value for L_D was estimated as the downwind distance from the leading edge of the vegetation to the midpoint between the pair of traps that produced the first negative sediment flux gradient after the maximum sediment flux value (Figure 3). L_c was estimated from Equation (4) using the most upwind anemometer data to determine C_D . The other parameters in Equation (4) were estimated from the vegetation geometry measurements made at the field sites (Table 1). We observed that the estimated length scales L_D and L_c migrated upwind as the vegetation cover and stem density increased.

3.2 | Empirical relationships between L_D and L_c

We were interested in determining the relationship between L_D and L_c such that the former could be estimated from the latter using a wide range of vegetation cover and wind speed values. To do this, we conducted a regression analysis on L_D and L_c using the Hesp et al.

(2019) laboratory dataset alone (Equation 11b) and the Hesp data with our field-determined values (Equation 11a). The regression analyses showed a significant positive linear relationship for L_D and L_c for both datasets (Figure 4; Equations 11b and 11a):

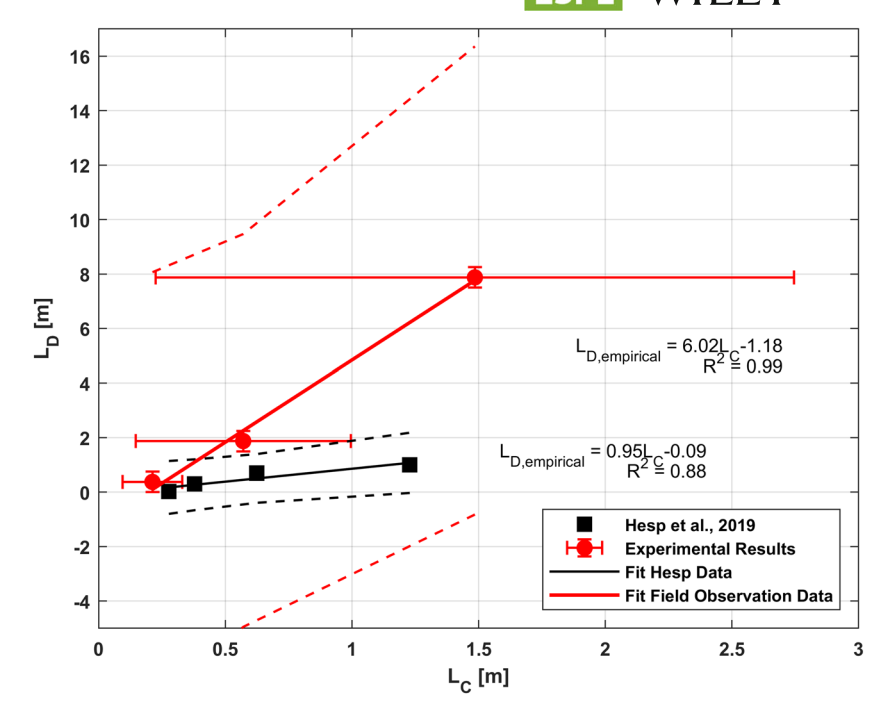
$$L_{D,empirical} = 0.95L_C - 0.09,$$
 (11a)

$$L_{D,empirical} = 6.02L_C - 1.18.$$
 (11b)

Equation (11a) was used for our Aeolis simulations of the Hesp et al. (2019) experiment and Equation (11b) was used for Aeolis simulations of field conditions, given that each equation produced the most realistic estimates of L_D and L_c for those separate applications of Aeolis.

3.3 | Aeolis modeling results for Hesp et al. (2019) laboratory wind tunnel experiment

To evaluate the performance of the Okin shear coupler and implementation of $L_{D,empirical}$ modifications into Aeolis, we modeled the development of the observed bedforms from the Hesp et al. (2019) wind tunnel experiment. Figure 5 shows the model results using both shear couplers with and without $L_{D,empirical}$. The Hesp et al. (2019) data show a decrease in bedform volume when the vegetation cover drops below the skimming flow regime and the bedform position (toe, crest, centroid, and heel) shifts downwind. The Raupach shear coupler produces errors in bedform volume that exceed 100% except for the 51% vegetation cover case (Figure 6a). However, even without $L_{D,empirical}$, the Okin shear coupler, using appropriate values for R_0 and



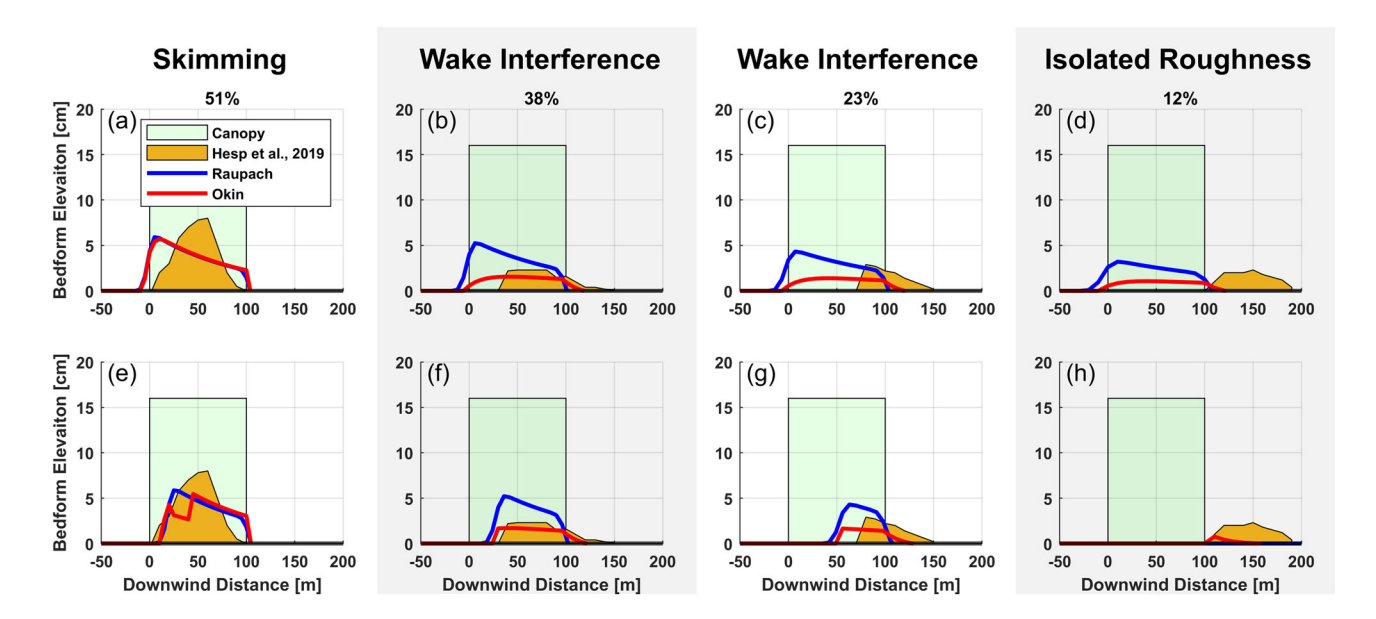


FIGURE 5 Bedforms modeled with Aeolis compared to observed bedforms from Hesp et al. (2019). Observed bedforms are shown in mustard and the canopy position in green. Model results from Raupach (blue) and Okin (red) in (a)–(d) do not include the deposition length scale. In (e)–(g) model results do include $L_{D,empirical}$. Vegetation cover and flow regime are written as a percentage above the corresponding column of figures [Color figure can be viewed at wileyonlinelibrary.com]

c for above and below 40% cover, reproduces the bedform volume to between 1% and 17% of the actual volume (Figure 6a). The improvement in bedform volume prediction is also shown through elevated BSS values for volume and elevation (Figure 7a,b). Neither shear coupler without the implementation of $L_{D,empirical}$ is able to reproduce the downwind shift in bedform toe location with decreasing vegetation cover (Figure 6c). However, the BSS values for the Okin shear coupler based on the bedform position of 0.35, 0.50, 0.64, and 0.25 for the 12%, 23%, 38%, and 51% vegetation cover cases indicate that the shear coupler does improve prediction of the bedform position for all cases even without implementation of $L_{D,empirical}$ (Figure 7c).

The inclusion of $L_{D,empirical}$ (Equation 11a) improves the bedform volume prediction using the Raupach shear coupler for all vegetation

cover cases except the 51% case (Figure 6b). The bedform volume prediction skill using the Okin shear coupler is lower with the inclusion of $L_{D,empirical}$; however, these predictions still have lower percent error than the predictions made using the Raupach shear coupler for all other vegetation cover cases (Figure 6b). The addition of $L_{D,empirical}$ allowed both shear couplers to produce the downwind shift in the bedform toe position with decreasing cover (Figure 6d). The biggest improvement in terms of position was accomplished using the Okin shear coupler with the $L_{D,empirical}$ expression, leading to position-based BSS values of 0.92, 0.90, 0.87, and 0.89 for the 12%, 23%, 38%, and 51% cover cases, respectively. In order to evaluate model skill relative to both position and volume, we considered the BSS computed by comparing the overall profiles (labeled as Elevation in Figure 7a),

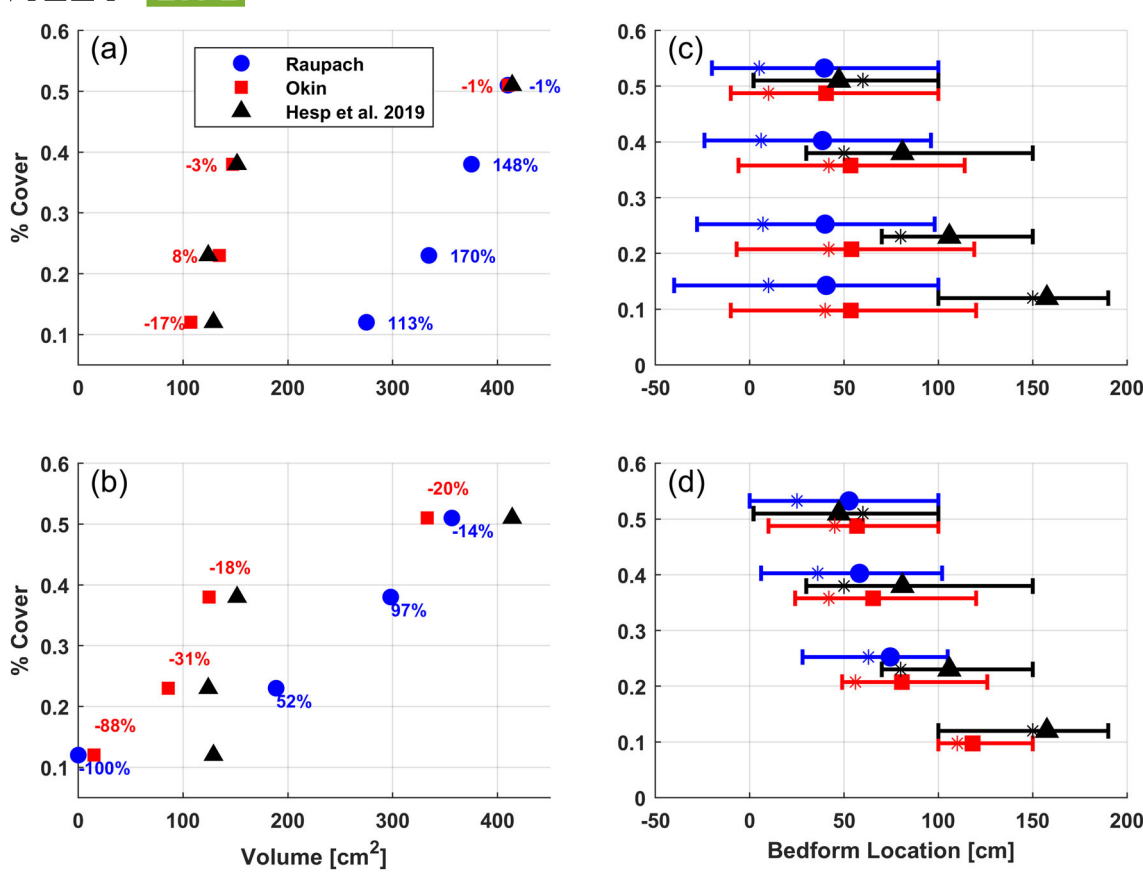


FIGURE 6 Comparison of Hesp et al. (2019) observations (black triangle) and the modeled bedform volumes and locations with the Raupach (blue circle) and Okin (red square) shear couplers using Aeolis. The left-hand column (a,b) shows bedform volumes computed without (top) and with (bottom) $L_{D,empirical}$. The percent error for each prediction is listed next the respective marker. The right-hand column (c,d) shows the bedform location with large marker at the centroid of the bedform; the bar extents indicate the toe and heel of the bedform. The star shows the horizontal location of the maximum bedform elevation [Color figure can be viewed at wileyonlinelibrary.com]

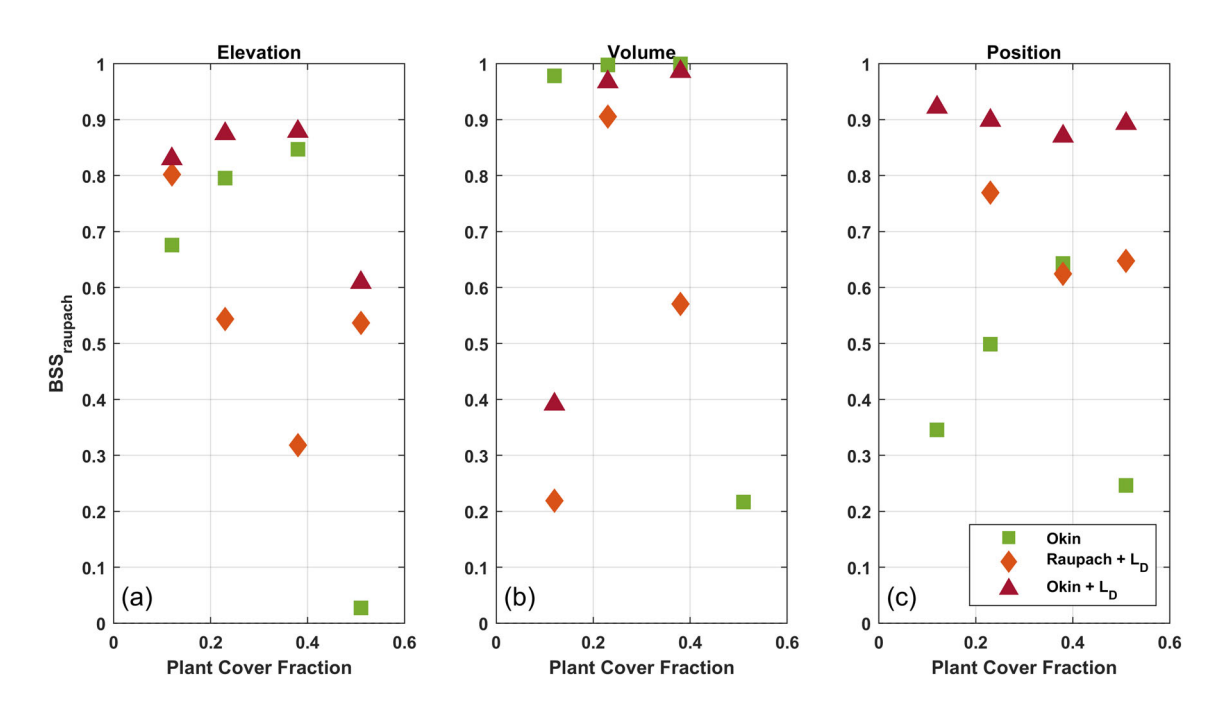
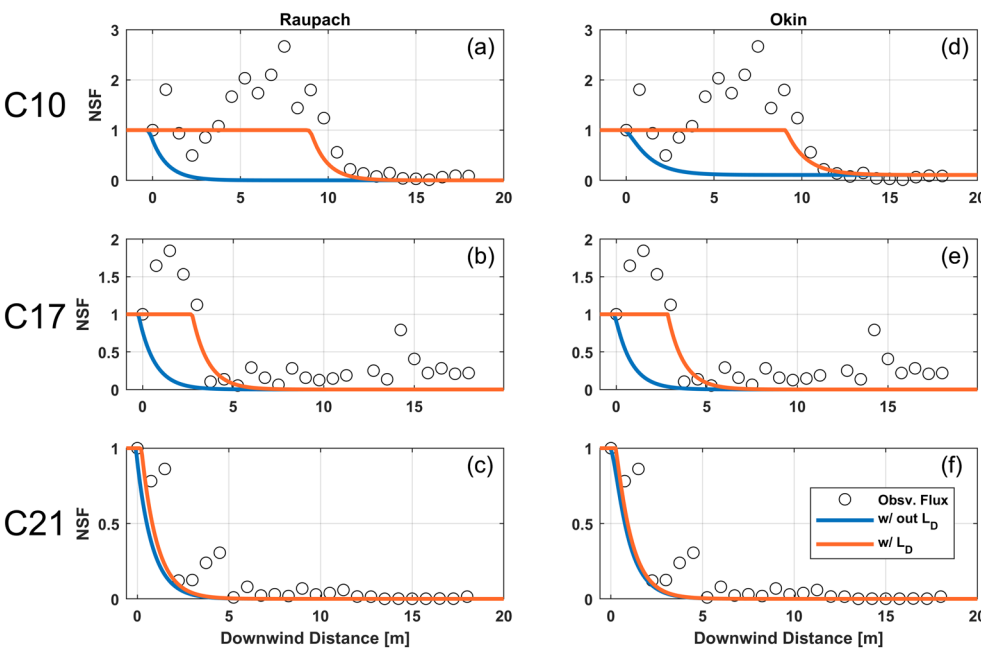


FIGURE 7 Brier skill scores for (a) 1D bed elevation, (b) bedform volume, and (c) bedform position, using three combinations of model modification (Okin, Raupach with $L_{D,empirical}$, Okin with $L_{D,empirical}$) relative to the baseline simulation with the Raupach shear coupler. All BSS values show improvement (positive value) with respect to the baseline Raupach simulation [Color figure can be viewed at wileyonlinelibrary.com]

FIGURE 8 Observed NSF (circle markers) compared to Aeolis model results with (orange line) and without L_D , empirical (blue line) for all three field transects (C10, C17, C21). The upwind sediment flux used for normalization of the model results is taken from x=-10 m because this location is within the region of the model domain where the sediment flux is assumed to be in equilibrium [Color figure can be viewed at wileyonlinelibrary.com]



which shows that the model using the Okin shear coupler with $L_{D,empirical}$ produces the most improvement in model skill for all cover cases, as indicated by BSS values of 0.83, 0.87, 0.61, and 0.88 for the 12%, 23%, 38%, and 51% cover cases, respectively.

3.4 | Aeolis modeling for field transect observations

The modeled NSF values from Aeolis simulations of the three field transects using $L_{D, \text{empirical}}$ from Equation (11b) are shown in Figure 8. $L_{D, \text{empirical}}$, based on vegetation cover and wind speed, adjusts the modeled downwind distance of the location where the sediment flux is attenuated below the upwind value (NSF < 1) to a distance closer to that observed in the field (circle markers).

The Raupach and Okin shear couplers without implementation of $L_{D,empirical}$ (Figure 8) similarly attenuate the sediment flux below 90% of the upwind value less than 1 m downwind of the canopy leading edge irrespective of transect. When $L_{D,empirical}$ is included, the downwind distance to the 90% attenuation point shifts downwind, providing a closer match with the field observations. For the Raupach shear coupler the 90% attenuation point shifts to 11.15, 4.82, and 2.24 m for transects C10, C17, and C21, respectively. Similarly for the Okin shear coupler, the 90% attenuation point shifts to >18, 4.91, and 2.30 m for transects C10, C17, and C21, respectively. The actual 90% attenuation points, according to our sediment flux measurements, are 12.75, 5.25, and 5.25 m for transects C10, C17, and C21, respectively. The two different shear couplers produce very similar results, with the exception that in the C10 case the Okin shear coupler never attenuates below 90% within the model domain. We see in Table 1 that the NSF value at $x = 18 \,\text{m}$ for the C10 case was observed to be 8.6E-02, while the Okin model including $L_{D,empirical}$ produced an NSF of 1.1E-01. These NSF values are of similar orders of magnitude indicating, while the model is overpredicting the sediment fluxes deep in the canopy, that the amount of attenuation produced by the model is realistic, in this case.

The BSS values shown in Figure 9 indicate that the Okin shear coupler alone provides a small improvement over the reference Raupach model for all vegetation cover values (BSS \leq 0.2). This illustrates that the shear stress recovery allowed within the canopy in the Okin expression does improve the model results for the range of vegetation covers in the three transects. Incorporating the empirical formulation for $L_{D,\text{empirical}}$ improves the model's ability to replicate the spatial distribution of the observed sediment fluxes relative to the reference model (BSS > 0), independent of which shear coupler is used (Figure 9). The Okin simulation including L_D exhibited the largest BSS values for all three cover cases, with 0.86, 0.21, and 0.10 for transects C10, C17, and C21, respectively. Note that for C21 both Okin and Okin + $L_{D,\text{empirical}}$ produce the same BSS value because $L_{D,\text{empirical}}$ is small at this vegetation cover value.

4 | DISCUSSION

Through field observations and analysis of an existing wind tunnel dataset, we found that sparse vegetation can have a non-local effect on aeolian sediment transport and deposition patterns. Modeling results demonstrate that the choice of shear coupler and inclusion of L_D , or the vegetation cover dependent deposition lag length downwind of sparsely vegetated dune grass canopies, improves the ability of Aeolis to predict morphological change in sparsely vegetated dune systems relative to predictions produced by current modeling practices.

4.1 | Evidence of a deposition lag in dune grass canopies

Although Hesp et al. (2019) did not quantitatively report on a deposition lag, these data have been reanalyzed here to suggest that there is a stem density/vegetation cover dependent role on L_D . This relationship suggests that high densities have almost no L_D , with sediment deposition occurring close to the leading edge of the patch. For

0969837, 2023, 5, Downloaded from https://onlinelibrary.wiley.com/doi/10.1002/esp.5526 by Oregon State University, Wiley Online Library on [12/02/2024]. See the Terms and Conditions (https://onlinelibrary.wiley.com/terms-and-conditions) on Wiley Online Library for rules of use; OA articles are governed by the applicable Creative Commons

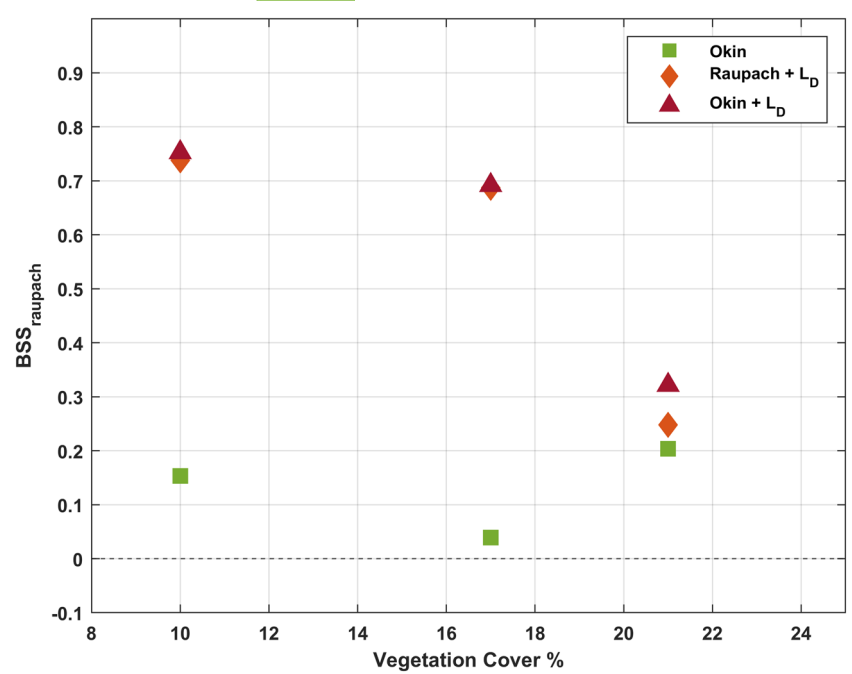


FIGURE 9 Brier skill score calculated based on the NSF values modeled for the vegetation cover of the three field transect simulations (transect C10 = 10% cover, transect C17 = 17% cover, and transect C21 = 21% cover) [Color figure can be viewed at wileyonlinelibrary.com]

vegetation cover less than the threshold for skimming flow (cover < 40%) we observe an increase in L_D with decreasing vegetation cover, for vegetation cover as small as 12%. The resulting relationship between L_D and L_c is closely approximated by a linear fit ($R^2 = 0.88$). The quality of this fit suggests a potential physical mechanism for L_D such that the distance to where deposition occurs appears to be related to the downwind distance required for flow to adjust to the canopy. A linear regression based only on the field data set also yields a strong fit ($R^2 = 0.99$) suggesting that our field observations again show that L_D depends on stem density/vegetation cover. The Hesp et al. (2019) and the field-derived datasets show different slopes between L_D and L_c . In general, the L_D values from the field datasets are longer than those from the laboratory, suggesting a potential dimensional scaling from laboratory scale to field scale. It should be noted that wind speeds, grain sizes, vegetation properties, and numerous other factors varied between the laboratory and field datasets. While we do not have the data necessary in our field study to estimate the roughness, Farrell and Sherman (2006) compared wind speed and sediment flux profiles from field and wind tunnel studies and found that the roughness was 6-7 times larger in field environments. Additionally, we cannot differentiate individual mechanisms or characteristics of the environment or vegetation that contribute to variability in L_D using our dataset because our observations are of an aggregation of all present characteristics. Despite differences in the slope and fit of L_D and L_c relationships depending on which dataset is used, the fact that both datasets (lab, field) and methods of collection (bed, flux) yield clear relationships with vegetation cover is broadly suggestive of the important role of stem density and plant morphology on non-local effects on bed shear stress, sediment transport, and deposition.

4.2 | Numerical modeling of sediment transport in vegetated dune canopies

We chose to use and improve the existing aeolian sediment transport model, Aeolis, for this study. As such, many of our choices and

discussions of model modifications are framed in the context of the existing Aeolis framework. Aeolis modifies the flow field as wind interacts with a canopy of vegetation using shear partitioning, or shear couplers. We kept consistent with this framework by adding a new shear coupler to Aeolis, and then modifying how the shear couplers modify the flow field using the proposed implementation of the vegetation drag length $L_{\rm D}$. Our observations of model improvement and limitations are outlined below.

4.2.1 | Limitations of current shear stress reduction approach

The Raupach shear coupler (Raupach, 1992) is widely used in landscape evolution models to parameterize the effects of vegetation and other roughness elements and their corresponding effects on bed shear stress, including numerous numerical models of coastal dune ecomorphodynamics (e.g., Durán & Moore, 2013; Hoonhout & de Vries, 2016; Roelvink & Costas, 2019). Typically, these models are run on grids with cell sizes of the order of meters and with a focus on timescales of months to decades. These spatial scales are generally greater than typical LD values found in the laboratory and field (e.g., Figure 4). As such, resolving L_D and the corresponding effect it has on deposition patterns may have little influence on morphological results for mesoscale studies with relatively coarse definitions of both morphology and vegetation properties. This could be especially true for cases with dense vegetation (e.g., >50%), as is characteristic of many natural coastal dune settings, where LD is small (Figures 4 and 5). It should also be noted that for cases with dense vegetation the Raupach shear coupler may also be invalid if the roughness density exceeds the limits established in Shao and Yang (2008).

However, for scenarios where vegetation is sparse—such as in many recently planted coastal dune settings—the spatial patchiness of vegetation may become increasingly important in determining the details of deposition patterns, which is also suggested by the findings of Okin (2008). In these sparsely vegetated scenarios, limitations of

ESPL-WILEY 919

the existing Raupach et al. (1993) approach become more apparent for both laboratory and field cases. Of course, utilizing either shear coupler approach ignores physical interaction, turbulent kinetic energy reduction, and other mechanisms that contribute to spatial changes in the sediment transport rate (Gillies et al.2018).

4.2.2 | Model improvement using L_D and Okin: Laboratory data

The Hesp et al. (2019) wind tunnel experiment was used to evaluate how the Okin shear coupler and the $L_{D,empirical}$ expression affect the model results. Our modeling results suggest that the Okin shear coupler improves the predicted bedform heel position across the entire range of stem densities (Figure 6). Similarly, incorporating the $L_{D,empirical}$ model improved the predicted position of the bedform toe (Figure 6). The model results suggest that $L_{D,empirical}$ greatly decreases the volume of sediment captured by the canopy regardless of the shear coupler used, which could be an artifact of the method for implementation in Aeolis, where shear reduction is masked over the $L_{D,empirical}$ length. If shear reduction was able to occur gradually over this length, the deposition volume decrease when using $L_{D,empirical}$ may not be as prevalent.

The values for R_0 (0.32) and c (4.8) recommended by Okin (2008) were based on observations of wind reduction in the lee of sand fences, which have properties that differ substantially from those of grasses. Therefore, these free parameters were calibrated using the 51% and 38% cover cases of Hesp et al. (2019). The calibrated values of R₀ found in this study unsurprisingly suggest a smaller initial reduction of the bed shear stress compared to the original values proposed by Okin (2008). Additionally, the trapped volume-based calibration procedure indicates that R₀ is inversely proportional to the cover percentage, resulting in a smaller initial reduction as the vegetation cover decreases. For the 51% cover case, the calibration method yielded a c value of 5.0, which is similar in magnitude to the published value (4.8). Consistent with Okin (2008), bed shear stress recovery is not immediate and takes place over some measurable length scale in the lee of plants or other obstacles to the wind field. However, the calibration procedure indicates that the length scale for recovery increases as canopy cover decreases, which is an unexpected outcome that may be related to the formation of individual wakes in canopies within the isolated roughness flow regime. The selection of R_0 and c for vegetation cover less than 40% resulted in Okin underpredicting volume for the model runs using L_D , indicating that these parameters may additionally be sensitive to properties of the canopy. Possible sensitivities in the determination of c may be related to the calibration approach. Values for R_0 and c were simply determined by minimizing the error in the trapped volume in the Hesp et al. (2019) wind tunnel study. However, the trapped volume is not linearly related to the shear reduction itself and is subject to any scaling issues that might be present in the wind tunnel configuration and/or limitations of the numerical model implementation (e.g., use of Bagnold-type sediment transport model). For the purposes of our study, it is assumed that these values for R_o and c derived from the flexible mimic vegetation experiments of Hesp et al. (2019) approximate those of natural dune grasses, at least more so than sand fences or rigid rods more commonly used for laboratory studies Additional wind tunnel studies or field observations of real vegetation are required to determine the values of R_0 and c for real vegetation over a range of densities.

The BSS indicates that both the Okin shear coupler and the $L_{D,empirical}$ expression improved model skill relative to the model using the Raupach shear coupler for the laboratory cases (Figure 7). This broad improvement in model skill suggests that the inclusion of $L_{D,empirical}$ and Okin can successfully resolve the dominant windvegetation interactions for sparsely vegetated dune grass canopies. However, it is also important to note that resolving these canopyscale dynamics requires grid resolutions ($\leq 0.1 \, \text{m}$) that are an order of magnitude finer than most ecomorphodynamic dune applications ($\sim 1 \, \text{m}$; Section 4).

4.2.3 | Modeling improvement using L_D and Okin: Field data

In the simulations of the field observations, the Okin shear coupler led to a small improvement, whereas inclusion of $L_{\text{D,empirical}}$ led to a large improvement in the prediction of the downwind location where sediment flux is attenuated below the flux upwind of the canopy leading edge (Figure 8). The improvement in field observation simulations using L_{D.empirical} is also evident from the BSS values, which increase as vegetation percent cover decreases (Figure 9). This indicates that the deposition lag effect is critical for correctly characterizing spatial patterns in sediment transport patterns and corresponding morphological changes associated with those transport gradients. The observations of the downwind distance to the point of 90% sediment flux attenuation and the model results shown in Figure 8 indicate that we tend to underestimate L_D with the $L_{D,empirical}$ linear regression. That said, the ability of the model using $L_{D, empirical}$ to represent the observed spatial patterns in sediment flux attenuation is encouraging. The ineffectiveness of Okin in improving the model skill in this application to the field transect observations is expected as the Okin shear coupler is mainly included to influence bedform geometry and volume, which we did not observe during our short deployments. However, the choice of shear coupler is not unimportant. Without L_D the model computed NSF values of 2.6E-09 and 1.1E-01 using the Raupach and Okin shear couplers, respectively, for transect C10 at $x = 18 \,\mathrm{m}$, where the value of the NSF measured in the field for transect C10 was 8.6E-02. When we compare these model results to the value for the sediment flux measured at $x = 18 \,\text{m}$ we see for transect C10 (the most sparse canopy) that the Okin shear coupler produces a better estimate of the flux deep within the canopy vegetation. The Hesp et al. (2019) dataset calibrated R_0 and c allow for larger fluxes within the canopy; the field observations suggest that R_0 and c should be tuned to allow for even greater amounts of transport within the canopy. This additional flux within the vegetation has implications for where deposition will occur. As an example, the ability of the Okin shear coupler to allow for appropriate levels of sediment flux within dune grass canopies of sparse vegetation is important for management scenarios in which the amount of sediment passing across the dune and subsequently inundating private property or public infrastructure (e.g., roadways, storm sewers) is an important consideration. Proper tuning of R_0 and c will allow for more accurate simulations.

The simulations of the transect field observations underpredict the sediment flux for transects C17 and C21. There are a number of factors that might explain why the model predictions do not exactly match the observed fluxes. To start, the duration of data collection is relatively short and covers a limited range of vegetation abundance, such that additional data would help ensure the quality of our empirical models for L_D . It is also important to note that the field observations occurred during the summer months, when wind speeds close to the threshold velocity can result in spatially and temporally intermittent transport. Observations of natural wind conditions have shown that temporally intermittent transport can be driven by gusts of wind such that transport occurs even when the mean wind speed is below the threshold of motion (Baas & Sherman, 2005; Lee, 1987; Stout & Zobeck, 1997). The aeolian sediment transport models used in our analysis assume continuous transport conditions. For this reason, time averages of the measured transport field were calculated from the available datasets for comparison to the models. A larger range of wind conditions could help inform any environmental dependence on the parameterizations for L_D .

Sediment flux is highly dependent on the bed shear stress, which in turn is dependent on velocity observations and assumptions about the local bed roughness. For this study we used the common assumption that the bed roughness, z₀, is dictated by the grain size (Sherman, 1992), which results in a $z_0 \approx 1E-5$ m. z_0 within the law of the wall is often representative of the roughness associated with boundary skin friction. It is possible that the z₀ is larger at individual sampling locations due to small-scale bedforms (i.e., ripples) and litter (e.g., plant debris). If the z_0 was increased from 1E-5 m to 1E-4 m, reflecting the role of these additional morphological elements, an order-ofmagnitude increase in sediment flux would be expected. Additionally, vegetation is often modeled as a form drag on the flow; however, Aeolis takes the approach of shear partitioning, which is a method to mimic the influence of form drag. Therefore, both z_0 and the methodology that Aeolis takes to model form drag from vegetation may explain some of the model-to-field data discrepancies.

Another factor affecting our transport predictions is the Bagnold coefficient, C_b , in Equation (5). The coefficient has traditionally been related to how well graded the grain size distribution is, with a larger coefficient being associated with a greater range of grain sizes (Bagnold, 1937). In our simulations of the transect field observations, we used a default value for the Bagnold coefficient of $C_b = 1.5$. However, modifying this transport constant is common when calibrating to specific site conditions (Sherman et al., 2013), in part due to uncertainty in the predictive skill of empirical models in coastal systems with a wide range of sediment supply limitations.

4.3 | Implications for modeling dune evolution across scales

We have demonstrated that the inclusion of L_D and the Okin shear coupler, depending on the values of coefficients R_0 and c, improves the predictive ability of Aeolis on the timescale of hours. In natural settings, the influence of L_D on model skill will be highest when dune grass canopies have low vegetation cover and diminish over time as vegetation naturally increases in density. The Hesp et al. (2019) wind tunnel experiment suggests that L_D goes to zero for vegetation cover greater than approximately 40%, which would correspond to the skimming flow regime proposed by Lee and Soliman (1977). Our field

observations showed that L_D was less than 1 m at $21\% \pm 9\%$ vegetation cover. In both cases we can see that there is some vegetation cover threshold where the length of LD decreases to the point that it would have limited impact on models of coastal foredune evolution. While we have not attempted to estimate the rate at which vegetation cover increases in sparse dune grass canopies, it is reasonable that L_D would become unimportant several years after management intervention and replanting due to natural vegetation growth and spread. It is also of note that this spatial scale is similar in size to grid spacing used in typical ecomorphodynamic dune modeling applications, thus minimizing the potential importance of L_D for cases with coarse grid resolution (dx < 1 m) and/or high vegetation cover. However, vegetation cover can vary considerably on dunes, leading to increases in L_D and therefore increasing its role in influencing corresponding aeolian deposition patterns. For example, overwash from extreme storms events can cause deposition within the dunes, resulting in an effective near-zero vegetation cover, and big wind events can bury vegetation, such that the effective canopy cover becomes much more sparse. In a less extreme example, seasonal periods of high winds can lead to high amounts of dune grass burial, which also have the effect of decreasing the canopy cover during the times of year when the most aeolian-driven morphological development occurs. Our model for L_D and the observations of Hesp et al. (2019) and Charbonneau and Casper (2018) suggest that these temporary reductions in vegetation cover lead to time periods where the importance of L_D increases. Longer term modeling studies and field observations are needed to evaluate seasonal variations in L_{D} and resulting impacts on morphological development.

5 | CONCLUSIONS

We have shown that the standard of practice (Raupauch shear coupler) used in models of aeolian processes to parameterize shear stress reduction from vegetation do not accurately predict the morphology within and downwind of sparse dune grass canopies. The use of the Okin shear coupler (Okin, 2008) and our newly proposed deposition lag length scale L_D are shown to improve the skill of modeling results with respect to both spatial patterns in sediment transport and volumetric morphological change within sparse dune grass canopies when implemented into the Aeolis model. The improvement in model skill relative to the standard modeling approach increases as canopy density decreases. By observing the downwind attenuation of wind speed and sediment flux in vegetation, we were able to extend the empirical expression for LD to account for sparse vegetation typical of newly planted managed dune systems. Future research is needed to investigate biophysical responses of a variety of dune plant species (Biel et al., 2019; Charbonneau et al., 2021; Hacker et al., 2012, 2019; Hesp, 1983; Zarnetske et al., 2012, 2015) and assess how well these models upscale to longer timescales in both natural and managed dune systems.

ACKNOWLEDGMENTS

We thank the Oregon Sea Grant under award number NA18OAR4170072 (CFDA No. 11.417) and the U.S. Army Corps of Engineers for funding field data collection and model application efforts. Aeolis model development carried out by N.C. and J.D. was supported by the U.S. Army Engineer Research and Development

-ESPL-WILEY 921

Center (ERDC) Coastal Inlets Research Program (CIRP) [Tools for Simulating Aeolian Transport] and Flood and Coastal Systems Research Program (F\&CS) [Resilience of Coastal Dunes] work units. The collection of field data was assisted by numerous individuals including Risa Askertooth, Nadia Cohen, Cecilia Girvin, Jessie Paskoski, John Stepanek, and Jeff Wood.

CONFLICT OF INTEREST

The authors declare that they have no conflicts of interest.

DATA AVAILABILITY STATEMENT

The data that support the findings of this study are freely available at https://zenodo.org.

ORCID

John Dickey https://orcid.org/0000-0001-5226-3468

Nicholas Cohn https://orcid.org/0000-0003-4287-039X

REFERENCES

- Avis, A.M. (1989) A review of coastal dune stabilization in the Cape Province of South Africa. *Landscape and Urban Planning*, 18(1), 55–68.
- Baas, A.C.W. & Sherman, D.J. (2005) Formation and behavior of aeolian streamers. *Journal of Geophysical Research: Earth Surface*, 110, F3.
- Bagnold, R.A. (1937) The Transport of Sand by Wind. *The Geographical Journal*, 89(5), 409-438.
- Barbier, E.B., Hacker, S.D., Kennedy, C., Koch, E.W., Stier, A.C. & Silliman, B.R. (2011) The value of estuarine and coastal ecosystem services. *Ecological Monographs*, 81(2), 169–193.
- Belcher, S.E., Harman, I.N. & Finnigan, J.J. (2012) The Wind in the Willows: Flows in Forest Canopies in Complex Terrain. Annual Review of Fluid Mechanics, 44(1), 479–504.
- Belcher, S.E., Jerram, N. & Hunt, J.C.R. (2003) Adjustment of a turbulent boundary layer to a canopy of roughness elements. *Journal of Fluid Mechanics*, 488, 369–398.
- Biel, R.G., Hacker, S.D. & Ruggiero, P. (2019) Elucidating Coastal Foredune Ecomorphodynamics in the U.S. Pacific Northwest via Bayesian Networks. Journal of Geophysical Research: Earth Surface, 124(7), 1919– 1938
- Biel, R.G., Hacker, S.D., Ruggiero, P., Cohn, N. & Seabloom, E.W. (2017) Coastal protection and conservation on sandy beaches and dunes: Context-dependent tradeoffs in ecosystem service supply. *Ecosphere*, 8(4), e01791.
- Bochev-van der Burgh, L.M., Wijnberg, K.M. & Hulscher, S.J.M.H. (2011) Decadal-scale morphologic variability of managed coastal dunes. Coastal Engineering, 58(9), 927–936.
- Bossard, V. & Nicolae Lerma, A. (2020) Geomorphologic characteristics and evolution of managed dunes on the South West Coast of France. Geomorphology, 367, 107312.
- Bradley, E.F. & Mulhearn, P.J. (1983) Development of velocity and shear stress distribution in the wake of a porous shelter fence. *Journal of Wind Engineering and Industrial Aerodynamics*, 15(1), 145–156.
- Brunet, Y., Finnigan, J.J. & Raupach, M.R. (1994) A wind tunnel study of air flow in waving wheat: Single-point velocity statistics. *Boundary-Layer Meteorology*, 70(1), 95–132.
- Buckley, R. (1987) The effect of sparse vegetation on the transport of dune sand by wind. *Nature*, 325(6103), 426–428.
- Charbonneau, B.R. & Casper, B.B. (2018) Wind tunnel tests inform Ammophila planting spacing for dune management, EarthArXiv.
- Charbonneau, B.R., Dohner, S.M., Wnek, J.P., Barber, D., Zarnetske, P. & Casper, B.B. (2021) Vegetation effects on coastal foredune initiation: Wind tunnel experiments and field validation for three dune-building plants. *Geomorphology*, 378, 107594.
- Chen, Z., Jiang, C. & Nepf, H. (2013) Flow adjustment at the leading edge of a submerged aquatic canopy. Water Resources Research, 49(9), 5537–5551.

- Cohn, N., Hoonhout, B., Goldstein, E., De Vries, S., Moore, L., Durán Vinent, O. & Ruggiero, P. (2019) Exploring Marine and Aeolian Controls on Coastal Foredune Growth Using a Coupled Numerical Model. *Journal of Marine Science and Engineering*, 7(1), 13.
- Cowles, H.C. (1899) The Ecological Relations of the Vegetation on the Sand Dunes of Lake Michigan. Part I.-Geographical Relations of the Dune Floras. *Botanical Gazette*, 27(2), 95–117.
- Luna, M.C.D.M., Parteli, E.J.R., Durán, O. & Herrmann, H.J. (2011) Model for the genesis of coastal dune fields with vegetation. *Geomorphology*, 129(3), 215–224.
- de Vries, S., van Thiel de Vries, J.S.M., van Rijn, L.C., Arens, S.M. & Ranasinghe, R. (2014) Aeolian sediment transport in supply limited situations. *Aeolian Research*, 12, 75–85.
- Durán, O. & Herrmann, H.J. (2006) Vegetation Against Dune Mobility. Physical Review Letters, 97(18), 188001.
- Durán, O. & Moore, L.J. (2013) Vegetation controls on the maximum size of coastal dunes. Proceedings of the National Academy of Sciences, 110(43), 17217–17222.
- Durán Vinent, O.F. & Moore, L.J. (2015) Barrier island bistability induced by biophysical interactions. *Nature Climate Change*, 5(2), 158–162.
- Farrell, E.J. & Sherman, D.J. (2006) Process-Scaling Issues For Aeolian Transport Modelling in Field and Wind Tunnel Experiments: Roughness Length and Mass Flux Distributions. *Journal of Coastal Research*, 2006, 384–389.
- Feagin, R.A., Figlus, J., Zinnert, J.C., Sigren, J., Martínez, M.L., Silva, R. et al. (2015) Going with the flow or against the grain? The promise of vegetation for protecting beaches, dunes, and barrier islands from erosion. Frontiers in Ecology and the Environment, 13(4), 203–210.
- Gadgil, R.L. & Ede, F.J. (1998) Application of scientific principles to sand dune stabilization in New Zealand: Past progress and future needs. *Land Degradation & Development*, 9(2), 131–142.
- Gillies, J.A., Etyemezian, V., Nikolich, G., Nickling, W.G. & Kok, J.F. (2018) Changes in the saltation flux following a step-change in macroroughness. Earth Surface Processes and Landforms, 43(9), 1871–1884.
- Gillies, J.A., Green, H., McCarley-Holder, G., Grimm, S., Howard, C., Barbieri, N. et al. (2015) Using solid element roughness to control sand movement: Keeler Dunes, Keeler, California. Aeolian Research, 18, 35–46.
- Gillies, J.A. & Lancaster, N. (2013) Large roughness element effects on sand transport, Oceano Dunes, California. *Earth Surface Processes and Landforms*, 38(8), 785–792.
- Gillies, J.A., Nickling, W.G. & King, J. (2006) Aeolian sediment transport through large patches of roughness in the atmospheric inertial sublayer. *Journal of Geophysical Research: Earth Surface*, 111, F2.
- Goldstein, E.B., Moore, L.J. & Durán Vinent, O. (2017) Lateral vegetation growth rates exert control on coastal foredune hummockiness and coalescing time. *Earth Surface Dynamics*, 5(3), 417–427.
- Hacker, S.D., Jay, K.R., Cohn, N., Goldstein, E.B., Hovenga, P.A., Itzkin, M. et al. (2019) Species-Specific Functional Morphology of Four US Atlantic Coast Dune Grasses: Biogeographic Implications for Dune Shape and Coastal Protection. *Diversity*, 11(5), 82.
- Hacker, S.D., Zarnetske, P., Seabloom, E., Ruggiero, P., Mull, J., Gerrity, S. & Jones, C. (2012) Subtle differences in two non-native congeneric beach grasses significantly affect their colonization, spread, and impact. Oikos, 121(1), 138–148.
- Hendriks, I.E., Sintes, T., Bouma, T.J. & Duarte, C.M. (2008) Experimental assessment and modeling evaluation of the effects of the seagrass Posidonia oceanica on flow and particle trapping. Marine Ecology Progress Series, 356, 163–173.
- Hesp, P.A. (1981) The Formation of Shadow Dunes. SEPM Journal of Sedimentary Research, Vol. 51.
- Hesp, P.A. (1983) Morphodynamics of Incipient Foredunes in New South Wales, Australia. In: Brookfield, M.E. & Ahlbrandt, T.S. (Eds.) Developments in Sedimentology. Eolian Sediments and Processes, Vol. 38, Elsevier, pp. 325–342.
- Hesp, P.A. (1989) A review of biological and geomorphological processes involved in the initiation and development of incipient foredunes. Proceedings of the Royal Society of Edinburgh, Section B: Biological Sciences, 96, 181–201.

- Hesp, P.A., Dong, Y., Cheng, H. & Booth, J.L. (2019) Wind flow and sedimentation in artificial vegetation: Field and wind tunnel experiments. Geomorphology, 337, 165–182.
- Hoonhout, B.M. & de Vries, S. (2016) A process-based model for aeolian sediment transport and spatiotemporal varying sediment availability:

 An Aeolian Sediment Availability Model. *Journal of Geophysical Research*: Earth Surface, 121(8), 1555–1575.
- Houston, J.A. & Jones, C.R. (1987) The Sefton Coast Management Scheme: Project and Process. *Coastal Management*, 15(4), 267–297.
- Jackson, N.L. & Nordstrom, K.F. (2011) Aeolian sediment transport and landforms in managed coastal systems: A review. Aeolian Research, 3(2), 181–196.
- Keijsers, J.G.S., Groot, A.V.D. & Riksen, M.J.P.M. (2016) Modeling the biogeomorphic evolution of coastal dunes in response to climate change. *Journal of Geophysical Research: Earth Surface*, 121(6), 1161– 1181.
- Lee, J.A. (1987) A field experiment on the role of small scale wind gustiness in aeolian sand transport. Earth Surface Processes and Landforms, 12(3), 331–335.
- Lee, B.E. & Soliman, B.F. (1977) An Investigation of the Forces on Three Dimensional Bluff Bodies in Rough Wall Turbulent Boundary Layers. *Journal of fluids engineering*, 99(3), 503–509.
- Martínez, M.L.M.L. & Psuty, N.P. (2008) Coastal dunes: Ecology and conservation, Ecological Studies, Vol. 171. Berlin; New York: Springer.
- Maun, M.A. (1998) Adaptations of plants to burial in coastal sand dunes. Canadian journal of botany, 76(5), 713–738.
- Miller, T.E., Gornish, E.S. & Buckley, H.L. (2009) Climate and coastal dune vegetation: Disturbance, recovery, and succession. *Plant Ecology*, 206(1), 97–104.
- Misak, R.F. & Draz, M.Y. (1997) Sand drift control of selected coastal and desert dunes in Egypt: Case studies. *Journal of Arid Environments*, 35(1), 17–28.
- Moore, L.J., Vinent, O.D. & Ruggiero, P. (2016) Vegetation control allows autocyclic formation of multiple dunes on prograding coasts. *Geology*, 44(7), 559–562.
- Munro, D.S. & Oke, T.R. (1975) Aerodynamic boundary-layer adjustment over a crop in neutral stability. Boundary-Layer Meteorology, 9(1), 53-61.
- Murphy, A.H. (1988) Skill Scores Based on the Mean Square Error and Their Relationships to the Correlation Coefficient. *Monthly Weather Review*, 116(12), 2417–2424.
- Nepf, H.M. (2011) Flow Over and Through Biota. In *Treatise on Estuarine* and Coastal Science, Elsevier, pp. 267–288.
- Okin, G.S. (2008) A new model of wind erosion in the presence of vegetation. *Journal of Geophysical Research*, 113(F2), F02S10.
- Olson, J.S. (1958) Lake Michigan Dune Development 2. Plants as Agents and Tools in Geomorphology. *The Journal of Geology*, 66(4), 345–351.
- Pickart, A. (1988) Overview: Dune Restoration in California: A Beginning. Restoration & Management Notes, 6(1), 8–12.
- Raupach, M.R. (1992) Drag and drag partition on rough surfaces. *Boundary-Layer Meteorology*, 60(4), 375–395.
- Raupach, M.R., Gillette, D.A. & Leys, J.F. (1993) The effect of roughness elements on wind erosion threshold. *Journal of Geophysical Research*: Atmospheres, 98(D2), 3023–3029.
- Reckendorf, F., Leach, D., Baum, R. & Carlson, J. (1985) Stabilization of Sand Dunes in Oregon. *Agricultural History*, 59(2), 260–268.
- Roelvink, D. & Costas, S. (2019) Coupling nearshore and aeolian processes: XBeach and duna process-based models. *Environmental Modelling & Software*, 115, 98–112.
- Rominger, J.T. & Nepf, H.M. (2011) Flow adjustment and interior flow associated with a rectangular porous obstruction. *Journal of Fluid Mechanics*, 680, 636–659.
- Ruggiero, P., Hacker, S., Seabloom, E. & Zarnetske, P. (2018) The Role of Vegetation in Determining Dune Morphology, Exposure to Sea-Level Rise, and Storm-Induced Coastal Hazards: A U.S. Pacific Northwest

- Perspective. In: Moore, L.J. & Murray, A.B. (Eds.) *Barrier Dynamics and Response to Changing Climate*. Cham: Springer International Publishing, pp. 337–361.
- Seneca, E.D., Woodhouse, W.W. & Broome, S.W. (1976) Dune stabilization with panicum amarum along the North Carolina coast. This Digital Resource was created from scans of the Print Resource.
- Shao, Y. & Yang, Y. (2008) A theory for drag partition over rough surfaces. *Journal of Geophysical Research: Earth Surface*, 113, F2.
- Sherman, D.J. (1992) An equilibrium relationship for shear velocity and apparent roughness length in aeolian saltation. *Geomorphology*, 5(3), 419–431.
- Sherman, D.J., Li, B., Ellis, J.T., Farrell, E.J., Maia, L.P. & Granja, H. (2013) Recalibrating aeolian sand transport models. Earth Surface Processes and Landforms, 38, 169–178.
- Sherman, D.J. & Nordstrom, K.F. (1994) Hazards of Wind-Blown Sand and Coastal Sand Drifts: A Review. Journal of Coastal Research, 1994, 263–275
- Sherman, D.J., Swann, C. & Barron, J.D. (2014) A high-efficiency, low-cost aeolian sand trap. Aeolian Research. 13, 31–34.
- Stout, J.E. & Zobeck, T.M. (1997) Intermittent saltation. *Sedimentology*, 44(5), 959–970.
- Sutherland, J., Peet, A.H. & Soulsby, R.L. (2004) Evaluating the performance of morphological models. *Coastal Engineering*, 51(8-9), 917–939.
- Van Westen, B. (2018) MSc_Thesis_Bart_van_Westen.pdf. Ph.D. Thesis.
- Wiedemann, A.M. & Pickart, A.J. (2004) Temperate Zone Coastal Dunes.
 In: Martínez, M.L. & Psuty, N.P. (Eds.) Coastal Dunes: Ecology and Conservation.
 Berlin, Heidelberg: Ecological Studies, Springer, pp. 53–65.
- Woodhouse, W.W. (1978) Dune building and stabilization with vegetation, Special Report (Coastal Engineering Research Center (U.S.)); No. 3. Coastal Engineering Research Center, U.S. Army, Corps of Engineers: Fort Belvoir, Virginia.
- Woodhouse, W.W. & Hanes, R.E. (1967) Dune Stabilization with Vegetation on the Outer Banks of North Carolina. U.S. Army, Coastal Engineering Research Center.
- Woodhouse, W.W., Seneca, E.D. & Broome, S.W. (1977) Effect of species on dune grass growth. *International Journal of Biometeorology*, 21(3), 256–266.
- Yang, J.Q., Chung, H. & Nepf, H.M. (2016) The onset of sediment transport in vegetated channels predicted by turbulent kinetic energy. Geophysical Research Letters, 43(21), 11,261–11,268.
- Zarnetske, P.L., Hacker, S.D., Seabloom, E.W., Ruggiero, P., Killian, J.R., Maddux, T.B. & Cox, D. (2012) Biophysical feedback mediates effects of invasive grasses on coastal dune shape. *Ecology*, 93(6), 1439–1450.
- Zarnetske, P.L., Ruggiero, P., Seabloom, E.W. & Hacker, S.D. (2015) Coastal foredune evolution: The relative influence of vegetation and sand supply in the US Pacific Northwest. *Journal of The Royal Society Interface*, 12(106), 20150017.
- Zong, L. & Nepf, H. (2010) Flow and deposition in and around a finite patch of vegetation. *Geomorphology*, 116(3), 363–372.

SUPPORTING INFORMATION

Additional supporting information can be found online in the Supporting Information section at the end of this article.

How to cite this article: Dickey, J., Wengrove, M., Cohn, N., Ruggiero, P. & Hacker, S.D. (2023) Observations and modeling of shear stress reduction and sediment flux within sparse dune grass canopies on managed coastal dunes. *Earth Surface Processes and Landforms*, 48(5), 907–922. Available from: https://doi.org/10.1002/esp.5526